Heliyon

Received:
20 February 2017
Revised:
9 August 2017
Accepted:
24 August 2017

Cite as: Becca Hoene, Dion Rivera. Optical studies of the solution phase reduction and stabilization of indigo tetrasulfonate in polyelectrolyte complexes. Heliyon 3 (2017) e00397. doi: 10.1016/j.heliyon.2017.e00397

Optical studies of the solution phase reduction and stabilization of indigo tetrasulfonate in polyelectrolyte complexes

Becca Hoene, Dion Rivera *

Department of Chemistry, Central Washington University, Ellensburg, Washington, 98926 United States

* Corresponding author.

E-mail address: riverad@cwu.edu (D. Rivera).

Abstract

Ultraviolet-visible (UV-vis) and fluorescence spectroscopy have been used to characterize the polyelectrolyte complexes (PECs) formed when potassium indigo tetrasulfonate (ITS) interacts with poly diallydimethylammonium chloride (PDADMAC) through columbic attraction in the presence of the reducing agent sodium bisulfite, $NaHSO_3$. The PDADMAC facilitates both the reduction of the ITS and the stabilization of the reduced state of the ITS in an atmospheric oxygen environment. Dilutions of the dye solution show that the PEC is stable to dilutions of at least 1 to 1000. UV–vis studies indicate that the reduced ITS (ITS_{red}) forms what is likely a J-aggregate in the presence of PDADMAC with an absorbance band red shifted from the normal absorbance band of reduced ITS by roughly 130 nm, 390 nm to 520 nm. Excitation of the PEC solution at either 390 nm or 520 nm produces an emission spectrum of the aggregated complex with an emission maximum near 534 nm. Monomer emission at 480 nm of ITS_{red} represents only 3.0 ± 0.5% of the emission signal of the aggregated complex. Kinetic studies using fluorescence spectroscopy over a temperature range of 30 to 70 °C and dilutions of dye solutions ranging from 1:10 to 1:1000 yield data for the oxidation of ITS_{red} that is best fit by a first order rate constant. Kinetic data displays two distinctive regimes, a short time rate and a long time rate. These two distinct kinetic regimes

http://dx.doi.org/10.1016/j.heliyon.2017.e00397

are likely due to the reduced ITS interacting with an outer PEC environment and an inner PEC environment. First order rate constants could be used to estimate $\Delta^{\ddagger}H$ and $\Delta^{\ddagger}S$ of the oxidation reaction. Fluorescence data was used to calculate the partitioning of reduced ITS molecules between the outer and inner PEC environments. Partitioning from the inner to outer PEC environment was found to be entropically driven. Addition of NaCl to the diluted dye solutions could alter the kinetics of the oxidation but the significance of the effect depended on the initial dye solution preparation.

Keywords: Materials chemistry, Physical chemistry

1. Introduction

Developing chemistries that can stabilize molecules in redox states that are not normally stable under atmospheric conditions has significant application for the indicator chemistry field [1, 2, 3]. Molecules whose color change can be controlled by redox or acid/base chemistry are particularly useful for packaging applications in the food and biomedical industries [1, 2, 3, 4, 5, 6, 7, 8, 9, 10, 11, 12, 13, 14, 15, 16, 17, 18, 19]. While many indicators are engineered to change color rapidly, there are applications for stabilization of the redox active species for long periods of time so that the color change is more gradual [1, 2]. Such applications include visual indicators on personal care consumer products that are meant to be used within a few hours of being exposed to atmospheric conditions and then disposed of or re-sterilized. This type of application requires a color change that is gradual enough to allow the device to be used within the appropriate time frame but shows a distinct color change once that time frame has expired.

Polyelectrolytes have been used in multiple applications including printing, coatings, water purification, and secondary oil recovery [20, 21, 22, 23, 24]. Polyelectrolytes have been used as protective coatings to prevent chemical degradation of underlying materials [25, 26], however, the use of polyelectrolyte chemistry to stabilize the redox states of molecules under environmental conditions that do not favor the oxidation state is quite novel. Polyelectrolytes have also been used to form colloidal structures that have cavities that act as so called "nanoreactors" that can catalyze chemical and biochemical reactions by concentrating the reactants in small volumes [27, 28, 29, 30]. To our knowledge, however, synthesis and stabilization of a reactive product in a nanoreactor type environment has not been reported.

Numerous studies have explored encapsulation of dye molecules by polyelectrolytes as model systems for waste removal and using the dye molecules to control macromolecular structures that have potential use in photo catalysis and solar energy applications [21, 23, 31, 32, 33, 34, 35, 36]. Some of these studies have employed polyelectrolyte/surfactant complexes created by oppositely charged

http://dx.doi.org/10.1016/j.heliyon.2017.e00397

polyelectrolytes and surfactants to encapsulate dye molecules in solution that are the same charge as the polyelectrolyte [37, 38]. More recently coacervate solutions have been shown to effectively sequester dye species [39]. These studies also indicate that the polyelectrolyte complex can be disrupted by changes in pH, ionic strength, and temperature. While the type of macromolecular complex may differ in these studies the common result is that under the correct conditions polyelectrolytes can form stable complexes in aqueous solutions that effectively sequester numerous types of dye molecules.

Recent work in our research group has shown that the redox dye indigo tetrasulfonate (ITS) can be reduced and stabilized in the reduced state in solutions of the polyelectrolyte polydiallydimethylammonium chloride (PDADMAC) in both the solution phase and as a thin film spread on plastic or cellulose materials as an ink [1, 2]. Using polyelectrolyte chemistry to both initiate redox chemistry and then stabilize the resulting redox state of a molecule both in solution and as a thin film is novel. In this manuscript, we report the solution phase kinetics of the oxidation of the redox dye ITS in solutions with the polyelectrolyte PDADMAC along with the entropy and enthalpies of activation. Spectroscopic data indicates the reduced ITS is aggregated in the PDADMAC to form a polyelectrolyte complex (PEC). The aggregated dye displays a significant red shift in absorbance and fluorescence that is characteristic of J-aggregate formation [40]. Additionally, the partitioning of ITS between the inner and outer environment at different temperatures is analyzed and the thermodynamic parameters of partitioning are presented.

2. Experimental

The materials used for the experiments were acquired from Sigma-Aldrich. The indigotetrasulfonate (ITS) had a specified dye content of 85%. Ethanol used in this study was 200 proof. A solution of 5% 2-hydroxyethyl cellulose (2HC), with an average molecular weight of 90,000 g/mol was used as a thickening agent. The PDADMAC solution was a 20 wt % aqueous solution with the molecular mass of the PDADMAC ranging from 400,000–500,000 g/mol. This corresponded to approximately 2474–3092 PDADMAC monomeric units. Sodium bisulfite ($NaHSO_3$) was ACS grade. Fig. 1 shows the structures of the ITS in the reduced and oxidized form along with the structures of PDADMAC and 2HC. All solutions were made with double reverse osmosis deionized water, conductivity > 17.5 MΩ.

Five different dye solutions were prepared with each solution containing 0.054 g of ITS, 10.47 g of ethanol, and 9.9 g of a 5% 2HC solution. This was allowed to mix for approximately 30 min under argon. For dye solution 1, 2.6 g of the 20% PDADMAC solution was added, and the solution allowed to mix overnight. After approximately 24 hours, 0.425 g of $NaHSO_3$ was added under argon and the ITS

http://dx.doi.org/10.1016/j.heliyon.2017.e00397

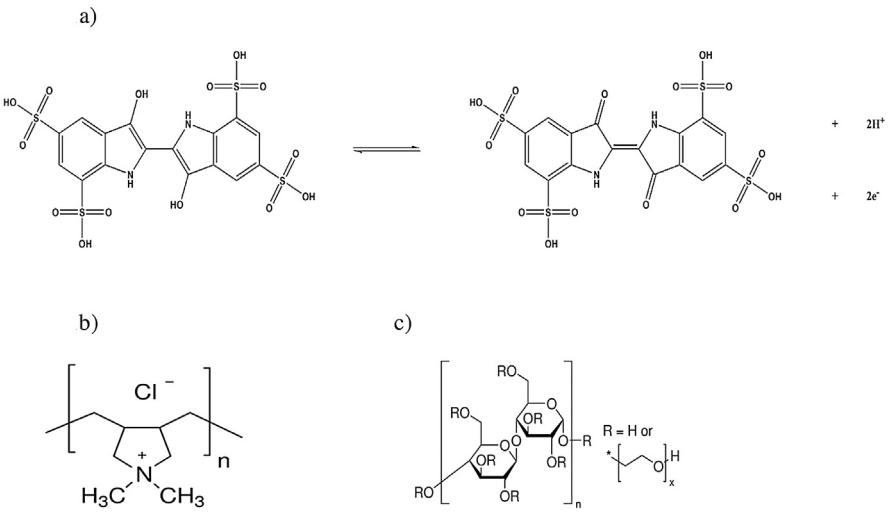

Fig. 1. a) Redox couple of ITS with the reduced form on the left and the oxidized form on the right (At the pH of the dye solutions used in this study the sulfonate groups on the ITS are deprotonated.). b) Monomeric unit of PDADMAC. c) Monomeric unit of 2HC.

turned from blue to yellow within 10 to 15 s. For dye solution 2, 1.3 g of the PDADMAC solution was used and for dye solution 3, 4.0 g of the PDADMAC solution was used. For dye solution 4 0.21 g of $NaHSO_3$ was used and for dye solution 5 0.64 g of $NaHSO_3$ was used. The mole ratios for ITS, PDADMAC monomer units, and $NaHSO_3$ for all dye solutions are summarized in Table 1. All dye solutions were stored in a glove box under argon and covered in Al foil when not in use. For experiments with increased ionic strength, NaCl (99.99%) was added to dilutions of dye solutions 3 and 5 so that the total NaCl concentration was 500 mM.

Ultraviolet-visible (UV-vis) spectrometry was used to characterize the absorbance spectrum for the various dye samples. A Hewlett-Packard 8453 UV–vis instrument and a quartz cuvette with a 1 cm path length were used. Fluorescence spectroscopy was used to measure the rate of the oxidation reaction occurring in the dye solutions. The instrument used was a Horiba FlouoroMax-4. The excitation

Table 1. Mole ratios of the ITS, PDADMAC monomer units, and sodium bisulfite in the dye solutions used in this study.

Dye Solution	Mole Ratio of ITS:PDADMAC$_{monmoer}$:$NaHSO_3$
1	1:218:56
2	1:109:56
3	1:327:56
4	1:218:27
5	1:218:84

http://dx.doi.org/10.1016/j.heliyon.2017.e00397

wavelength was set to 520 nm, with emission readings taken in the range of 525–700 nm. The slit width was set to 1 nm for both excitation and emissions. Short time scans were taken over a period of 6.5 min with a time resolution of 28 s, and long time scans were taken over a period of 3.4 h with a time resolution of 208 s. The linear range of the instrument was found to be from 500 to 3,100,000 counts per second (CPS). If scans were taken that exceeded that range, a neutral density filter was added in order to reduce the CPS to the linear range of the instrument.

Fluorescent studies were conducted at the following temperatures: 30 °C, 40 °C, 50 °C, 60 °C, and 70 °C. A VWR Scientific 1136 water circulator was used to ensure that the temperature was constant for the length of the experiment, with a variation of ± 0.1 °C. The partial pressure of oxygen in all studies was 0.20 ± .01 atm.

Solution pH measurements of the 1:10 dilutions of each ink system were taken with a sympHony SP70 P pH meter. A three point calibration was conducted with buffer solutions of pH 4.00, 7.00, and 10.00. The pH measurements for 1:10 dilutions of dye solutions 1 to 5 are 3.34, 3.42, 4.06, 3.10, and 3.23 respectively. The pH of 1 to 100 and 1 to 1000 dilutions of the dye solutions yields a pH in the 5.0 to 6.0 range.

Dissolved oxygen (DO) readings were taken using a YSI 550A DO meter. The calibration was set to an altitude of 1600 feet and a solution salinity of 0.0 mg/L. Experiments were done in the 1:10, 1:100, and 1:1000 dilutions of dye solution 1 in the absence of the indicator molecule, ITS. The first DO reading for each trial was taken after bubbling the solution with argon gas and subsequent measurements were taken after the minimum DO concentration was determined. DO readings for the 1:10 dilution were recorded every 208 s for approximately 3.4 h, or 60 cycles, in order to get a similar time resolution to that of the fluorescent decay readings taken on the fluorimeter. For all other dilutions only the initial ($t = 0$ s) and final ($t = 3.4$ h) DO concentrations were recorded. Even with the presence of $NaHSO_3$ and argon purging, all solutions registered measurable levels of dissolved oxygen shown in Table 2. All solutions have significantly less DO than control solutions, 6.25 to 6.50 mg/L.

Table 2. Concentration of dissolved oxygen in dye 1 solution.

Dilution of Solution with concentrations of components equivalent to dye solution 1	Initial dissolved oxygen concentration (mg/L)	Dissolved oxygen concentration after 3.4 h (mg/L)
1:10	0.51	0.84
1:100	1.55	3.27
1:1000	1.25	2.87

http://dx.doi.org/10.1016/j.heliyon.2017.e00397

3. Results and discussion

All dye solutions were a simplification of the ink formulations given in reference 1 where ethanol and 2-hydroycellulose are added as an aid in the drying of the ink and as a rheological modifier respectively. This formulation was chosen as the stock solution for the dye solutions so that the resulting kinetic information can be related back to chemistries that occur in the ink type solutions. Even when left open to atmospheric concentrations of oxygen for several weeks these dye solutions show very limited oxidation of the ITS. Due to the slow nature of the oxidation of the ITS_{red} in the stock dye solutions and the desire to understand the stability of the PEC in diluted solutions, all kinetic studies were carried out on diluted dye solutions with dilutions ranging from 1:10 to 1:1000. These dilutions provide a more reasonable time scale for studying the kinetics of the ITS oxidation.

Fig. 2 shows the UV–vis adsorption spectra of dye solution 1 before and after the addition of sodium bisulfite. The absorbance band in Fig. 2a at 590 nm is the absorbance of the oxidized ITS and agrees with the literature [5, 41]. Fig. 2b shows strong adsorption by the reduced ITS (ITS_{red}) around 390 nm in agreement with the literature and a band with a λ_{max} at 520 nm that has not been reported in the literature. The absorption band at 520 nm is attributed to the formation of a J-aggregate type structure (see discussion below). Dye solutions made without the addition of PDADMAC do show that 20% of the ITS can be reduced with addition of bisulfite but the reduced ITS is not stabilized in these dye solutions. This is illustrated in Fig. 3 showing the UV–vis spectra of diluted dye solution 1 after exposure to the atmosphere for approximately 10 min with and without PDADMAC added. Fig. 3 clearly shows that the ITS is completely reduced with the addition of PDADMAC and that the ITS_{red} is stabilized by the presence of PDADMAC as no absorption bands for the ITS_{red} are seen in the spectrum with no PDADMAC added. Experiments titrating bisulfite into dye solutions show that the PDADMAC produces complete reduction of the ITS at bisulfite concentrations ~80 times lower than without the presence of PDADMAC. Additionally, dye solutions with PDADMAC present show very slow oxidation kinetics of ITS under atmospheric conditions, on the order of weeks, compared to solutions with no PDADMAC present. Presence of PDADMAC is also critical to controlling the rate of oxidation of ink films that turn from the reduced yellow color to an oxidized blue color [1, 2]. The PDADMAC therefore plays a significant role in reducing and stabilizing the ITS_{red}.

Fig. 4 shows that fluorescence excitation at 390 nm and 520 nm of the reduced ITS dye solutions produce very similar fluorescence spectra with an emission maximum near 534 nm. Emission maximum for ITS_{red} has been reported at 485 nm with a 385 nm excitation [5]. Emission maximum of the ITS_{red} observed at 534 nm represents a ~ 0.23 eV red shift of the emission. The fluorescence signal at 534

http://dx.doi.org/10.1016/j.heliyon.2017.e00397

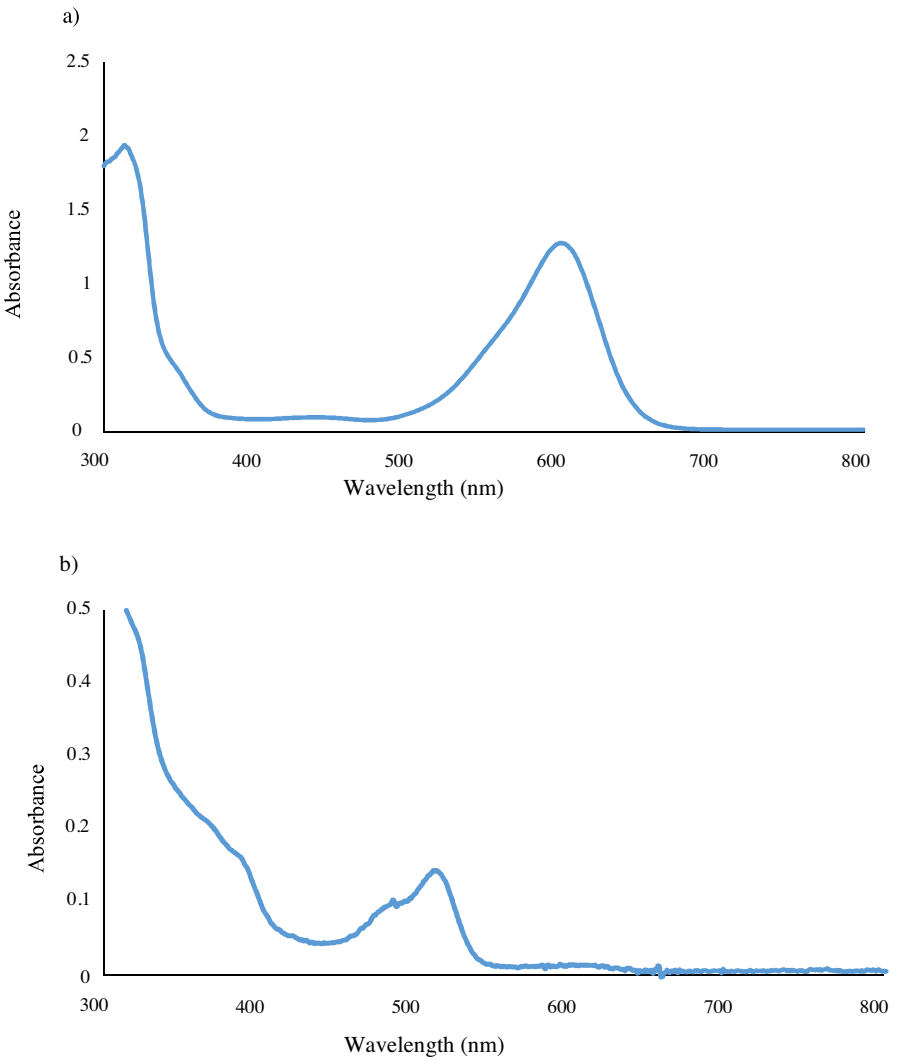

Fig. 2. a) Absorbance readings of a 1:10 dilution of dye solution 1 before addition of bisulfate. b) A 1:50 dilution of dye solution 1 after addition of bisulfite. The large absorbance near 300 nm is due to the matrix of the dye solution.

nm is present at dilutions of the dye solution of 1:1000 at long times after the solution has been exposed to oxygen, see Fig. 4c (the small band at 450 nm in Fig. 4c is due to water Raman). This data clearly shows that the addition of PDADMAC red shifts the emission spectra of the ITS_{red} relative to environments with no ITS present. Dyes that complex with macromolecules are known to form so called J-aggregates that show large shifts in the absorption and fluorescence spectra of the dye and can increase in the fluorescence intensity [31, 32, 33, 34, 40]. Dye molecules similar to ITS have been shown to interact strongly with polyelectrolytes and have shown a reduction in the fluorescence intensity of bands due to monomers and an increase in excimer bands as the PDADMAC concentration is increased [42]. Aggregation of the dye molecules within the

http://dx.doi.org/10.1016/j.heliyon.2017.e00397

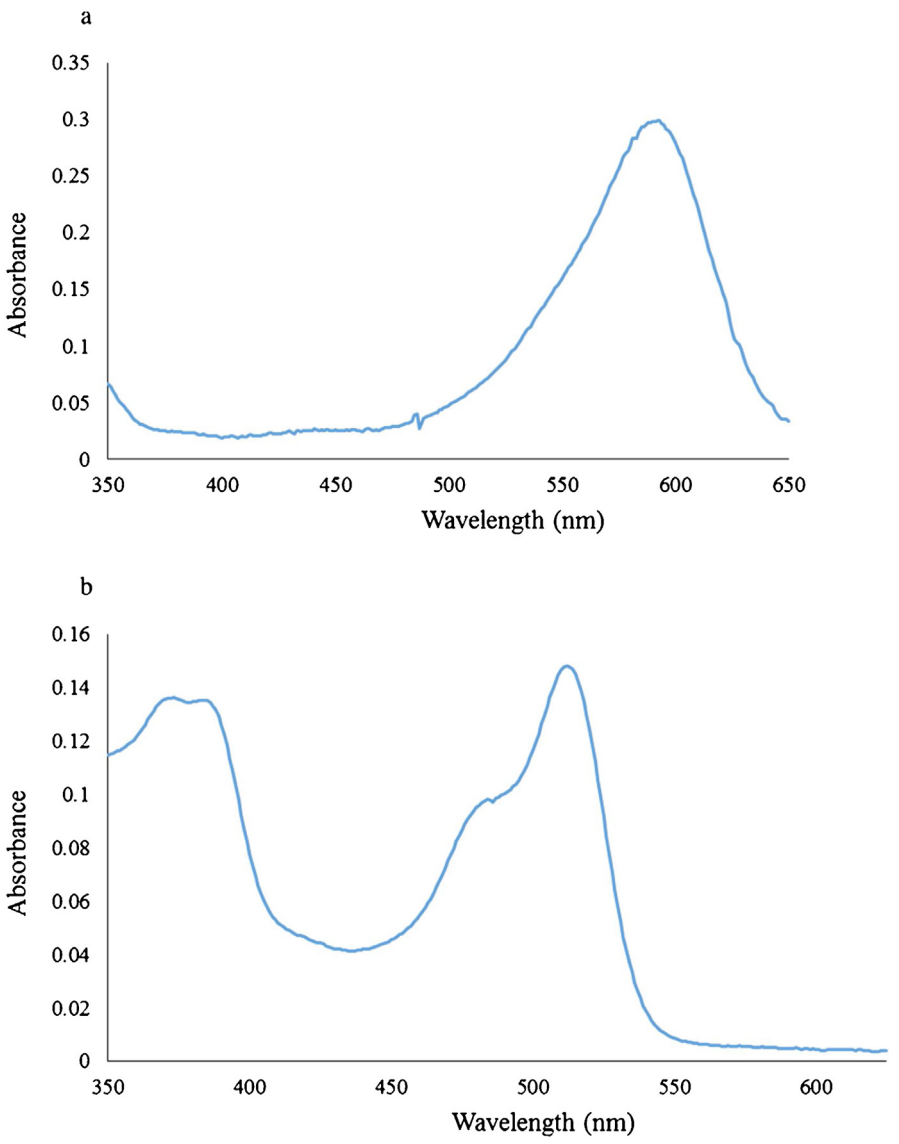

Fig. 3. Absorbance spectra of 1:50 dilutions of dye solution 1 after approximately 10 min exposure to the atmosphere. A) Diluted dye solution 1 with no PDADMAC added. B) Diluted dye solution 1 with PDADMAC present.

PEC causes π-π interactions between adjacent dye molecules that leads to a delocalization of the electrons within the dyes conjugated system that leads to a lower energy absorption band [31, 32, 33, 34, 40]. Given the strong red shift, ~0.8 eV, relative to the 390 nm monomer absorption band, both the absorption band centered at 520 nm and the corresponding fluorescence band at 535 nm are assigned to an aggregated structure of the reduced ITS within the PDADMAC. Experiments in this study utilized the excitation at 520 nm since this band is sensitive solely to the aggregated structure and only probes the aggregated ITS_{red} within the PEC.

http://dx.doi.org/10.1016/j.heliyon.2017.e00397

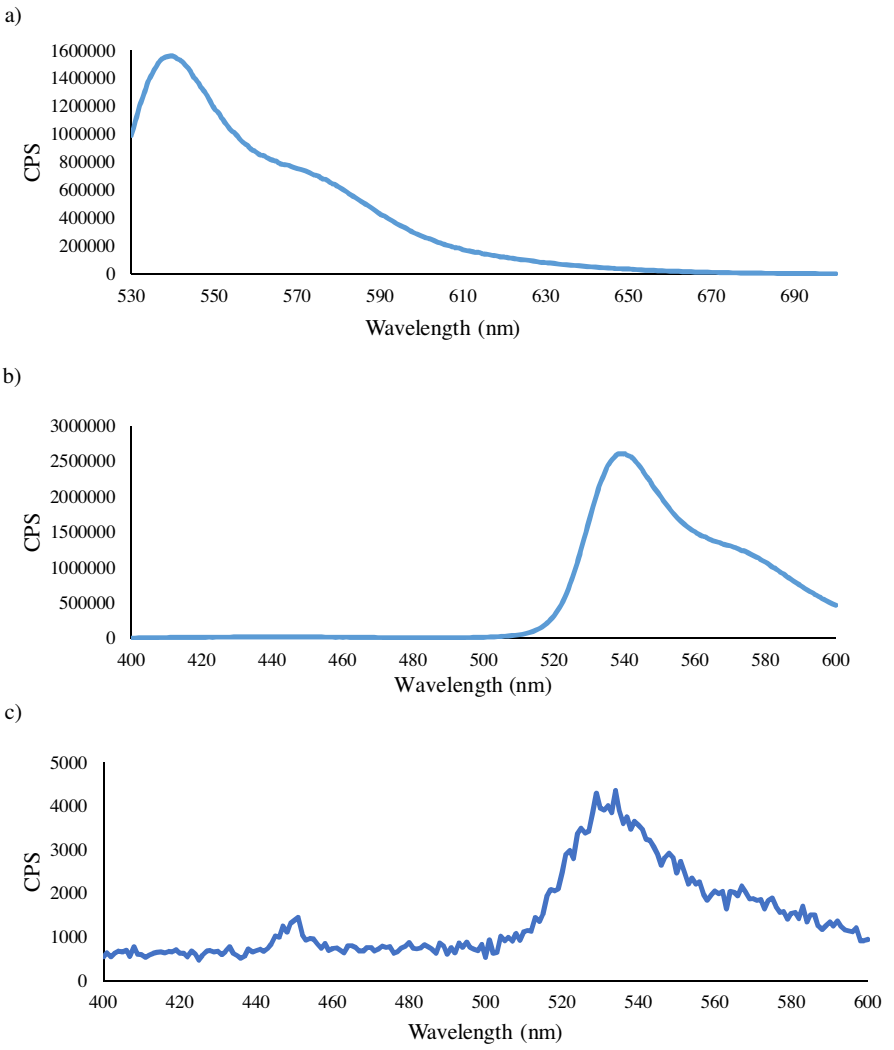

Fig. 4. a) Fluorescence emission of a 1 to 10 dilution of ink solution 1 with 520 nm excitation. b) Fluorescence emission of a 1 to 10 dilution of ink solution 1 with 390 nm excitation. c) Fluorescence emission of a 1 to 1000 dilution of ink solution 1 with 390 nm. excitation after exposure to oxygen for 1 h. Y-axis values are in counts per second (CPS) and the absolute emission intensity has not been corrected for the neutral density filters used.

The monomer fluorescence is not significant in these samples, 3.0 ± 0.5% of the aggregate ITS_{red} emission, indicating that a significant majority of ITS_{red} is interacting with the PDADMAC in an aggregated complex. The absorption of photons at 390 nm indicates that some fraction of the ITS_{red} molecules undergo an adsorption process at the monomer adsorption λ_{max} but the excited state emission is primarily as the aggregate indicating that ITS_{red} molecules that undergo adsorption at 390 nm are interacting in an aggregated structure associated with the PEC. It could be argued that monomer ITS_{red} molecules are adsorbing the radiation and emitting photons that are re-adsorbed by aggregated ITS_{red} molecules. Given

http://dx.doi.org/10.1016/j.heliyon.2017.e00397

efficiency of the emission seen at 534 nm relative to 480 nm emission for adsorption at 390 nm the mechanism of re-adsorption would still require any monomer molecules to surrounded by the aggregated species.

Fig. 5 shows the fluorescence of dye solution 1 with 525 nm excitation with and without bisulfite added. Essential no fluorescence is seen in the solution without the addition of bisulfite indicating that the observed fluorescence is from the ITR_{red}. The ITS_{red} species has been identified as the fluorescent species in the literature [5]. Fig. 6 shows the fluorescence spectra of dye solution 1 prepared with and without PDADMAC added after exposure to atmospheric oxygen for approximately 10 min. Essentially no fluorescence is seen in the solution with no PDADMAC added but a very strong fluorescence signal is seen in the solution with PDADMAC added. This data further supports the importance of the role of PDADMAC in stabilizing the ITS_{red}.

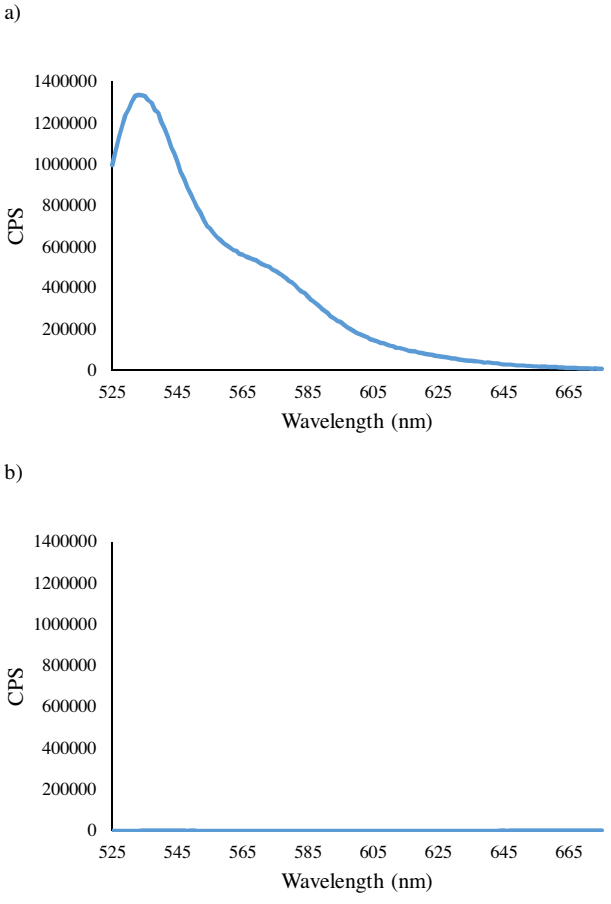

Fig. 5. a) Fluorescence readings a 1:100 dilution of dye solution 1 with excitation at 520 nm after reduction with bisulfite. b) Fluorescence readings of the solution in a) with an excitation wavelength of 520 nm before reduction with bisulfite. The y-axis values are in counts per second (CPS) and the absolute emission intensity has not been corrected for the neutral density filters used.

http://dx.doi.org/10.1016/j.heliyon.2017.e00397

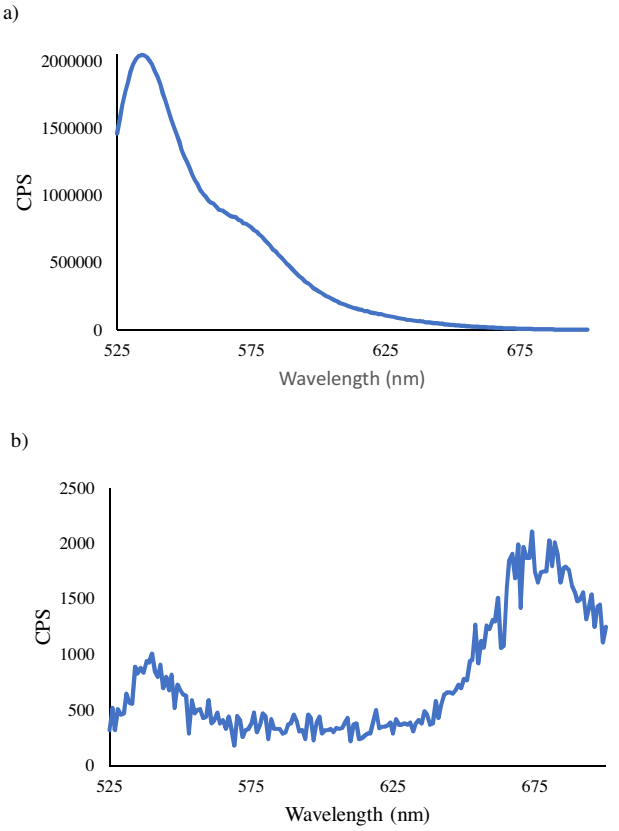

Fig. 6. a) Fluorescence spectra of a 1 to 100 dilution of dye solution 1 containing PDADMAC with excitation at 520 nm. b) Fluorescence spectra of a 1 to 100 dilution of dye solution 1 containing no PDADMAC with excitation at 520 nm. Solutions were exposed to the atmosphere for approximately 10 min.

Typical time dependent fluorescence spectra of ITS dye solution 1 at 30 and 70 °C are shown in Fig. 7 for the 1 to 10 dilutions acquired over 3.4 h (see Experimental section). Fig. 8 shows the fluorescence decay of the reduced ITS signal at 534 nm with time. It can clearly be seen from Fig. 8 that two distinct kinetic regimes exist. Nearly all data follows this trend for all dye solutions, dilutions, and temperatures used in this study. The exception is the 1 to 10 dilutions of the dye solutions at 30 and 40 °C that display an increase in the fluorescence output during the long time studies (see later discussion). The data presented in Fig. 4 indicates that all detectable emission for excitation of ITS_{red} at 520 nm probes only the aggregated complex and therefore the decrease in the reduced form of the ITS is due to oxidation of the ITS molecules in the aggregated complex. The two distinct kinetic regions indicate that two distinct environments exist for the ITS molecules interacting with the PDADMAC. These environments will be referred to as an outer PEC environment that is described by the shorter time kinetic component and an inner PEC environment that is described by the longer time kinetic component.

http://dx.doi.org/10.1016/j.heliyon.2017.e00397

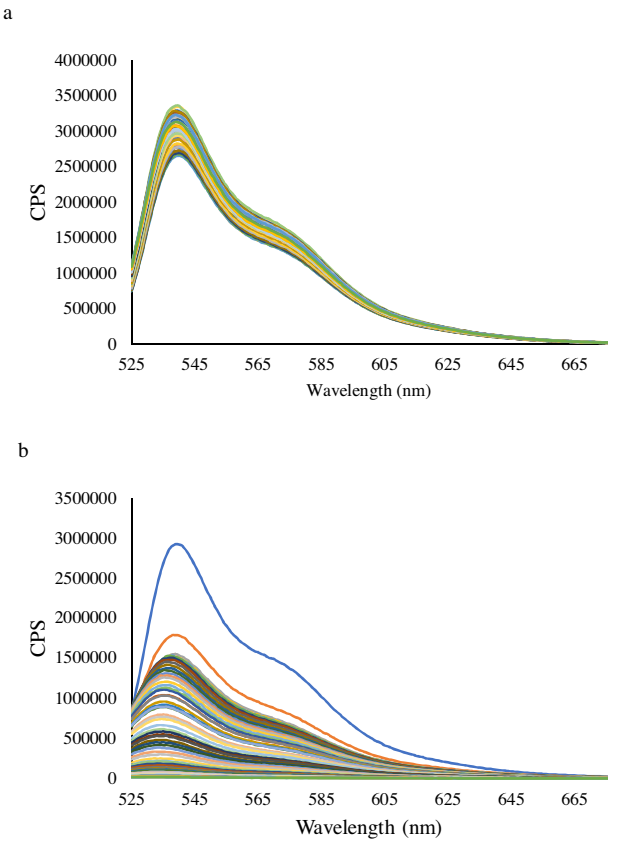

Fig. 7. a) Fluorescent change of long time scans of the 1:10 dilution of dye solution 1 at 30 °C. b) Fluorescent change of long time scans of the 1:10 dilution of dye solution 1 at 70 °C. The uppermost peak represents the scan taken starting at time 0 s and the lower most peak represents the final scan. The y-axis values are in counts per second (CPS) and the absolute emission intensity has not been corrected for the neutral density filters used.

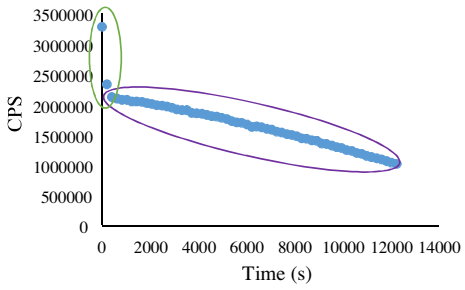

Fig. 8. Fluorescent intensity change at 534 nm of Ink A. The green ellipse corresponds to the short scans and the purple ellipse corresponds to the long scans. The y-axis values are in counts per second (CPS).

http://dx.doi.org/10.1016/j.heliyon.2017.e00397

Since fluorescence of the ITS monomer is not significant the reaction of any monomer ITS with oxygen is assumed to be diffusion limited and not the rate limiting step of the oxidation process. Literature also suggests a very rapid oxidation of monomeric ITS with low concentrations of oxygen in solution [5, 41].

Bisulfite is the other negatively charged species in the system and 90 to 95% of the unreacted bisulfite would exist as HSO_3^- in solution at the initial pH of the dye solutions used in this study. The columbic interactions between the PDADMAC and the negatively charged ITS and bisulfite can create microenvironments within the PEC, as shown in Fig. 8, that significantly increase the local concentration of bisulfite relative to PDADMAC (mole ratios of ITS to bisulfite vary from 1:27 to 1:84 in the ink solution used in this study). The high concentration of bisulfite in this microenvironment drives the reduction of the ITS and the high concentration HSO_3^- in the microenvironment protects the ITS from oxidation by dissolved oxygen in the dye solution. Chemical reactions of the HSO_3^- with ITS_{ox} and O_2(aq) are given below:

$$HSO_3^- (aq) + ITS_{(ox)} (aq) + H_2O \rightarrow ITS_{(red)} (aq) + HSO_4^- (aq) \quad (1)$$

$$2HSO_3^- (aq) + O_2 (aq) \rightarrow 2HSO_4^- (aq) \quad (2)$$

Oxidation of ITS with dissolved oxygen is given below:

$$O_2 (aq) + 2ITS_{red} (aq) \rightarrow 2ITS_{ox} (aq) + 2H_2O (l) \quad (3)$$

Fig. 9 depicts an environment where the ITS_{red} is loosely interacting with the PDADMAC in an outer environment and an inner environment where the ITS_{red} is strongly associated with the PDADMAC. The ITS_{red} in the outer environment would more exposed to oxygen dissolved in the solution and would be in an environment with a reduced bisulfite concentration. The ITS_{red} in the outer environment would be more easily oxidized. This outer environment is not considered free solution since the aggregated ITS_{red} complex is being probed with 520 nm excitation. The ITS_{red} in the inner environment would not be able to interact with dissolved oxygen as readily and would likely be in an environment with a higher bisulfite concentration. These two microenvironments would yield the two distinct kinetic regimes for the oxidation of ITS_{red} seen in the data and are treated as the two distinct chemical reactions given below:

$$½\ O_2 (aq) + PDADMAC(ITS_{red})_{outer} (aq) \rightarrow PDADMAC(ITS_{ox})_{outer} (aq) + H_2O (l) \quad (4)$$

$$½\ O_2 (aq) + PDADMAC(ITS_{red})_{inner} (aq) \rightarrow PDADMAC(ITS_{ox})_{inner} (aq) + H_2O (l) \quad (5)$$

Since there was a clear distinction in the two kinetic regimes the data analysis was split into a short time component, the first 240 s, and a long time component, 240 s to the end of the analysis. The data was found to follow first order kinetic behavior

 http://dx.doi.org/10.1016/j.heliyon.2017.e00397

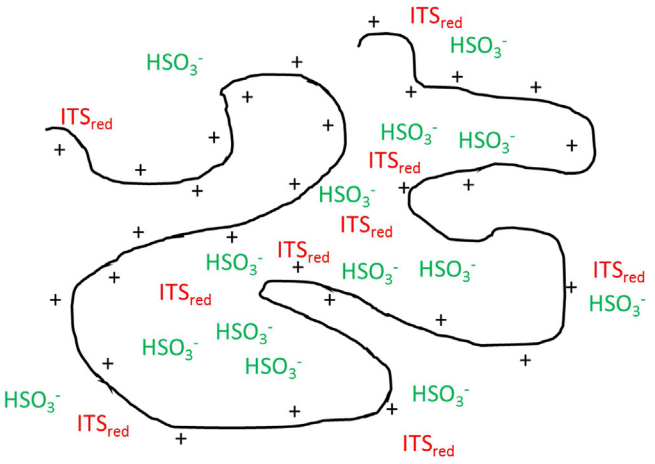

Fig. 9. Cartoon depicting the outer PEC environment where the reduced ITS (ITS_{red}) molecules interact with a more open environment and the inner PEC environment that is less open and contains a higher local concentration of bisulfite ion.

in the loss of ITS_{red}. The decrease of fluorescence for both the long time component and short time component was modeled using the first order integrated rate law shown below:

$$[ITS]_{red} = -kt + [ITS]_{red0} \quad (6)$$

where t is time in seconds, k is the first order rate constant, $[ITS]_{red}$ is the concentration of reduced ITS at a given time, and $[ITS]_{red0}$ is the initial concentration of the reduced ITS. Fluorescence for the short time kinetic experiments was corrected for the contribution from the long time fluorescence component by estimating the fraction of ITS_{red0} in the inner complex from the long time data and using that to correct for the $[ITS]_{red0}$ present in the inner complex.

The kinetic analysis outlined above implicitly assumes that variation in the populations of ITS_{red} molecules in the inner and outer environment for a given dilution of a dye solution is negligible over the time frame of the experiments. Diffusion of ITS_{red} between the inner and outer environments undoubtedly occurs on the time scale of the experiments but the kinetic analysis outlined above fits the data well (see below) and there is little indication that diffusion between the environments significantly alters the populations of the ITS_{red} in the inner and outer environments. Diffusion in confined spaces such as the inner complex is quite slow when strong molecular interactions are involved due to the low probability the of a molecule finding a path that is free of the attractive forces [43]. Polyelectrolytes are known to form very stable complexes with oppositely charged molecules under the right conditions and therefore it is most likely the inner complex tightly binds the ITS_{red} molecules making the rate of diffusion between the inner and outer environments much slower than the oxidation of the ITS_{red}.

http://dx.doi.org/10.1016/j.heliyon.2017.e00397

The rate constants obtained over the temperature range of 30 to 70 °C were used to calculate the $\Delta^{\ddagger}H$ and $\Delta^{\ddagger}S$ of the activated complex for the rate limiting step of the reaction using the Eyring equation [44] given below:

$$\ln(k/T) = -\Delta^{\ddagger}H/RT + \ln(k_B/h) + \Delta^{\ddagger}S/R \quad (7)$$

where k is the first order rate constant, R in the ideal gas constant, T is the temperature, k_B is the Boltzmann constant, and h is Plank's constant. In this case a graph of 1/T verses ln(k/T) yields a slope of $-\Delta^{\ddagger}H/R$ and an intercept equivalent to $\ln(k_B/h) + \Delta^{\ddagger}S/R$. This analysis assumes that any back reaction, $ITS_{ox} \rightarrow ITS_{red}$, would be insignificant compared to the forward reaction. Use of the Eyring equation for the electron transfer reaction $ITS_{red} \rightarrow ITS_{ox}$ is consider a valid model since bonds are being broken and formed during the chemical reaction allowing the transition state to be modeled as an activated complex.

Sodium bisulfite can react with certain ketones and aromatic alcohols to add a sulfonic acid or amine [45, 46]. The potential reactions of bisulfite with the alcohol or ketone functionality would destroy the conjugation of the system and result in a dye that displays blue shifted absorbance bands. However, all optical spectroscopy data indicates that the absorption bands of ITS are maintained during the experiments. The oxidized ITS displays the same absorbance maximum at the end of the experiments as it did prior to the addition of bisulfite. Creation of amine functionality under the aqueous environment used in the preparation of dye solutions is unlikely as the reactants, ITS and HSO_3^-, would be favored in this reaction.

Additionally, ITS is the highest sulfonated derivative in the indigo dye family. Literature president for the existence of a penta sulfonate indigo dye could not be found. An oxidation reduction reaction between bisulfite and ITS as outline in equations 1 and 2 is the most likely reaction pathway under the experimental conditions and is in agreement with the spectroscopic data.

Tables 3, 4, 5, 6, 7 and 8 show the first order kinetic rate constants for the outer PEC environment for all dye solutions. The correlation coefficients (R^2) are given as an assessment of the linearity of the data but not a validation of the first order model. Fits of the data to higher order integer rates or fractional order rate constants did not result in better modeling of the data as determined by chi squared analysis at the 95 percent confidence interval. Apparent first order behavior is expected since the concentration of the bisulfite is 24 to 72 times greater than the concentration of the ITS depending on the dye solution and pseudo first order behavior in the rate of the oxidation of the ITS_{red} is expected. The applicability of the first order model even at dilutions of 1:1000 of the dye solutions indicates that ITS_{red} still exists in the outer environment of the PEC despite the dilutions.

Tables 3, 4, 5, 6 and 7 do show a consistent pattern of the first order rate constant increasing by 1 to 2 orders of magnitude as the dye solution become more dilute.

http://dx.doi.org/10.1016/j.heliyon.2017.e00397

Table 3. Short time kinetic data for dye solution 1. R^2 values are the square of the correlation coefficient for the fit of the kinetic data to the first order model.

Temperature °C	First Order Rate Constant for 1 to 10 Dilution (s^{-1})	First Order Rate Constant for 1 to 100 Dilution (s^{-1})	First Order Rate Constant for 1 to 500 Dilution (s^{-1})	First Order Rate Constant for 1 to 1000 Dilution (s^{-1})
30	5.4×10^{-3} $R^2 = 0.943$	9.4×10^{-3} $R^2 = 0.991$	7.2×10^{-4} $R^2 = 0.936$	6.6×10^{-3} $R^2 = 0.993$
40	4.1×10^{-3} $R^2 = 0.988$	6.7×10^{-3} $R^2 = 0.999$	2.3×10^{-3} $R^2 = 0.983$	1.2×10^{-2} $R^2 = 0.962$
50	1.0×10^{-2} $R^2 = 0.993$	1.1×10^{-2} $R^2 = 0.997$	4.0×10^{-3} $R^2 = 0.931$	1.5×10^{-2} $R^2 = 0.955$
60	6.2×10^{-3} $R^2 = 0.994$	1.1×10^{-2} $R^2 = 0.995$	5.1×10^{-3} $R^2 = 0.955$	3.5×10^{-2} $R^2 = 0.962$
70	6.5×10^{-3} $R^2 = 0.982$	1.1×10^{-2} $R^2 = 0.998$	9.6×10^{-3} $R^2 = 0.956$	3.6×10^{-2} $R^2 = 0.959$

Increase in the first order rate constant indicates that the outer environment of the PEC becomes more open with increasing dilution. This more open environment is less protective of the ITS_{red} and results in a more rapid rate of oxidation of the ITS. However, even at the average value for the first order rate of oxidation of the ITS_{red} at 70 °C for the 1:1000 dilution of dye solutions 1–3, 2.7×10^{-2} s^{-1}, the half-life is 25.7 s. In free solution, the rate of oxidation of ITS_{red} is essentially diffusion limited and given that the dissolved O_2 concentration is roughly 5 to10 times greater than the total ITS_{red} concentration in the 1:1000 dilution (see Table 2) the rate of oxidation is still significantly slower in the outer PEC environment compared to what is expected in free solution [5, 41].

Kinetic rates for the short time data do not consistently fit the temperature dependent rate model given in equation 7. This is likely due to a greater partitioning of bisulfite to the outer environment as temperature is increased. Partitioning of ITS_{red} between the inner and outer environments increases as the temperature increases (see latter discussion) and it is reasonable to assume that more bisulfite also partitions to the outer PEC environment. Mole ratios of ITS to bisulfite vary from 1:27 to 1:84 across the dye solutions so the local concentration

Table 4. Short time kinetic data for dye solution 2. R^2 values are the square of the correlation coefficient for the fit of the kinetic data to the first order model.

Temperature °C	First Order Rate Constant for 1 to 10 Dilution (s^{-1})	First Order Rate Constant for 1 to 100 Dilution (s^{-1})	First Order Rate Constant for 1 to 500 Dilution (s^{-1})	First Order Rate Constant for 1 to 1000 Dilution (s^{-1})
30	3.9×10^{-4} $R^2 = 0.951$	6.8×10^{-3} $R^2 = 0.981$	1.3×10^{-2} $R^2 = 0.966$	1.2×10^{-2} $R^2 = 0.987$
40	4.6×10^{-4} $R^2 = 0.980$	1.1×10^{-2} $R^2 = 0.996$	1.8×10^{-2} $R^2 = 0.938$	1.8×10^{-2} $R^2 = 0.969$
50	2.4×10^{-3} $R^2 = 0.997$	1.1×10^{-2} $R^2 = 0.997$	2.4×10^{-2} $R^2 = 0.966$	2.0×10^{-2} $R^2 = 0.968$
60	3.1×10^{-3} $R^2 = 0.992$	9.8×10^{-3} $R^2 = 0.999$	2.7×10^{-2} $R^2 = 0.972$	1.8×10^{-2} $R^2 = 1.00$
70	4.4×10^{-3} $R^2 = 0.994$	1.3×10^{-2} $R^2 = 0.997$	2.7×10^{-2} $R^2 = 0.990$	2.4×10^{-2} $R^2 = 0.990$

http://dx.doi.org/10.1016/j.heliyon.2017.e00397

Table 5. Short time kinetic data for dye solution 3. R^2 values are the square of the correlation coefficient for the fit of the kinetic data to the first order model.

Temperature °C	First Order Rate Constant for 1 to 10 Dilution (s^{-1})	First Order Rate Constant for 1 to 100 Dilution (s^{-1})	First Order Rate Constant for 1 to 500 Dilution (s^{-1})	First Order Rate Constant for 1 to 1000 Dilution (s^{-1})
30	6.1×10^{-4} $R^2 = 0.963$	2.6×10^{-3} $R^2 = 0.999$	5.1×10^{-3} $R^2 = 0.980$	1.6×10^{-2} $R^2 = 0.994$
40	5.7×10^{-4} $R^2 = 0.958$	2.3×10^{-3} $R^2 = 0.996$	1.1×10^{-2} $R^2 = 0.993$	1.3×10^{-2} $R^2 = 0.995$
50	1.1×10^{-3} $R^2 = 0.980$	3.6×10^{-3} $R^2 = 0.999$	1.5×10^{-2} $R^2 = 0.994$	1.4×10^{-2} $R^2 = 0.994$
60	1.7×10^{-3} $R^2 = 0.990$	5.9×10^{-3} $R^2 = 0.998$	2.6×10^{-2} $R^2 = 0.937$	1.6×10^{-2} $R^2 = 0.982$
70	3.2×10^{-3} $R^2 = 0.989$	8.6×10^{-3} $R^2 = 0.997$	2.6×10^{-2} $R^2 = 0.973$	2.1×10^{-2} $R^2 = 0.982$

of ITS in the outer environment increases significantly as the temperature is increased. This leads to deviations in the expected temperature dependence of the rate constants.

While there is not a consistent temperature dependence of the rate constants for the inner PEC environment, data from Tables 3, 4, 5, 6 and 7 that do display a temperature dependence can be fit to equation 7. This analysis is caveated by the fact that the ITS_{red}:HSO_3^- ratio in the outer environment may not be consistent over the temperature range modeled. Average $\Delta^{\ddagger}H$ and $\Delta^{\ddagger}S$ values across all kinetic data for the outer PEC environment that display a temperature dependence that can be fit to equation 7 are 41 ± 10 kJ/mol and −130 ± 30 J/molK respectively. It is interesting to note that studies of spherical ionic macromolecules and dyes with a −3 charge have a Gibbs free energy of interaction of −39 to −44 kJ/mol [35]. This interaction value is very close to the activation enthalpies in the outer PEC environment. The rate limiting step of oxidation of ITS_{red} in the outer PEC environment may be the disruption of the attractive forces between ITS_{red} and PDADMAC.

Table 6. Short time kinetic data for dye solution 4. R^2 values are the square of the correlation coefficient for the fit of the kinetic data to the first order model.

Temperature °C	First Order Rate Constant for 1 to 10 Dilution (s^{-1})	First Order Rate Constant for 1 to 100 Dilution (s^{-1})
30	1.6×10^{-3} $R^2 = 0.988$	9.5×10^{-3} $R^2 = 0.975$
40	5.3×10^{-3} $R^2 = 0.970$	9.9×10^{-3} $R^2 = 0.997$
50	8.8×10^{-3} $R^2 = 0.996$	8.4×10^{-3} $R^2 = 0.999$
60	8.1×10^{-3} $R^2 = 0.996$	9.2×10^{-3} $R^2 = 0.999$
70	9.5×10^{-3} $R^2 = 0.997$	1.0×10^{-2} $R^2 = 0.999$

http://dx.doi.org/10.1016/j.heliyon.2017.e00397

Table 7. Short time kinetic data for dye solution 5. R^2 values are the square of the correlation coefficient for the fit of the kinetic data to the first order model.

Temperature °C	First Order Rate Constant for 1 to 10 Dilution (s^{-1})	First Order Rate Constant for 1 to 100 Dilution (s^{-1})
30	3.8×10^{-3} $R^2 = 0.947$	1.2×10^{-2} $R^2 = 0.966$
40	7.5×10^{-3} $R^2 = 0.997$	7.5×10^{-3} $R^2 = 0.996$
50	7.4×10^{-3} $R^2 = 0.990$	9.9×10^{-3} $R^2 = 0.999$
60	7.3×10^{-3} $R^2 = 0.979$	9.8×10^{-3} $R^2 = 0.998$
70	6.6×10^{-3} $R^2 = 0.979$	1.1×10^{-3} $R^2 = 0.996$

First order rates of dye solutions 3 and 5 at 1:10 dilution with 500 mM NaCl added are shown in Table 8. The higher ionic strengths of these solutions would be expected to provide more shielding between the PDADMAC and the ITS in the outer environment resulting in very weak electrostatic attraction between the two molecules and less stability in the ITS aggregates in the outer environment. The first order rate constants of dye solution 3 with NaCl added increase as the temperature increases, however, the relative increase in the rate constant decreases as the temperature approaches 70 °C. Dye solution 5 shows more complex behavior. Addition of 500 mM NaCl to dye solution 5 at 30 °C results in a rate that is roughly 5 times greater than without salt added but increasing the temperature results in a decreased reaction rate. Dye solution 5 contains 50% more HSO_3^- than dye solution 3 and this increased ionic strength of dye solution 5 appears to influence the PEC that is formed.

Results of the short time kinetic analysis give a picture of the outer complex environment where the ITS_{red} is exposed to a more open environment with increasing temperature. However, the outer environment of the complex does not completely break apart even at 70 °C and dilutions of 1:1000. This indicates that the columbic interactions between the ITS_{red} and the PDADMAC are significant in

Table 8. Short time kinetic data for dye solution 3 and 5 in a 500 mM NaCl solution. R^2 values are the square of the correlation coefficient for the fit of the kinetic data to the first order model.

Temperature °C	First Order Rate Constant for 1 to 10 Dilution (s^{-1}) for Dye Solution 3	First Order Rate Constant for 1 to 10 Dilution (s^{-1}) for Dye Solution 5
30	5.0×10^{-4} $R^2 = 0.982$	2.0×10^{-2} $R^2 = 0.960$
40	1.0×10^{-3} $R^2 = 0.997$	9.6×10^{-3} $R^2 = 0.992$
50	2.2×10^{-3} $R^2 = 0.995$	3.4×10^{-3} $R^2 = 0.999$
60	3.3×10^{-3} $R^2 = 0.999$	4.3×10^{-3} $R^2 = 0.996$
70	4.7×10^{-3} $R^2 = 0.999$	5.9×10^{-3} $R^2 = 0.996$

http://dx.doi.org/10.1016/j.heliyon.2017.e00397

the outer PEC environment. These columbic interactions can be disrupted by increasing the ionic strength of the solution which leads to a more open structure in the outer environment of the PEC.

PECs that were formed in higher ionic strength dye solutions can display decreased reaction rates as the temperature is increased, see Table 8. Additionally, 1:10 dilutions display significant variance in the kinetic behavior as a function of temperature. This result is counter intuitive, however, the reason for this behavior is likely due to an increase in the number of bisulfite molecules in the outer environment as the temperature is increased. Partitioning coefficients, see latter discussion, show that the concentration of ITS_{red} in the outer environment increases with temperature and higher ionic strength. This is due to the disruption of the inner environment of the PEC. While the spectroscopic studies do not directly detect the concentration of bisulfite in the different environments, it is reasonable to expect that the concentration of bisulfite in the outer environment would also increase as temperature increases. As the mole ratios of the ITS to bisulfite vary from 1:27 to 1:84 for the various dye solutions it is expected that the concentration of bisulfite in the outer environment would be significantly greater than the concentration of the ITS_{red} in the outer environment. Increases in the concentration of bisulfite would cause the measured rates to deviate from the expected behavior with increasing temperature. Deviations would be most pronounced at 1:10 dilutions of the dye solution as the bisulfite concentration in the inner environment is greatest and less pronounced at the 1:500 and 1:1000 dilutions. This is essentially the trend presented in the kinetic data though changes in the PDADMAC concentration complicates the picture as the increased PDADMAC concentration changes the number of binding sites for ITS and bisulfite.

The release of bisulfite from the inner PEC environment would also explain why the rate of ITS_{red} oxidation decreases with increasing temperature at the 1:10 dilution for dye solution 5 with 100 mM NaCl added. This dye solution contains 50% more bisulfite than dye solution 4 so that when the PEC is formed more bisulfite will be sequestered in the inner environment than would occur with dye solution 4. As the system is heated and more bisulfite is released to the outer environment, increasing the concentration of bisulfite in the outer environment and preventing oxygen from reacting with ITS_{red} as rapidly as would be expected. Both dye solutions with NaCl added show the fraction of ITS_{red} in the outer environment to be ~0.80 at 70 °C, see latter discussion, so the concentration of bisulfite in the outer environment would also be expected to be quite high. Dye solution 3 with NaCl added does not display this behavior due to both a lower concentration of bisulfite and higher concentration of $PDADMAC_{monmer}$, $ITS:PDADMAC_{monomer}$ of 1:218 and 1:335 for dye solution 3 and 5 respectively with NaCl added. This

http://dx.doi.org/10.1016/j.heliyon.2017.e00397

combination effectively dilutes the concentration of bisulfite in the outer environment of the PEC as the solution is heated.

Kinetic data for the oxidation of ITS in the inner PEC environment for 1:10 dilutions of the dye solutions are more complicated than the more dilute solutions. The 1:10 dilutions show an increase in the florescence intensity at 30 and 40 °C for the long time scans. For the scans above 40 °C the fluorescence intensity decreases with time as would be expected. Experiments with control solutions (all components except ITS present) at the same concentration show that none of the other components yield this fluorescence profile. Therefore, it is likely the increase in the fluorescence signal rises from a back reaction of $ITS_{ox} \rightarrow ITS_{red}$. This phenomenon is not apparent in the more diluted dye samples due to the dilution of the bisulfite. It is likely that the concentration of the bisulfite within the inner environment of the PEC of the 1:10 dilutions is sufficiently high to re-reduce oxidized ITS that has been created in the inner environment. This also explains why the fully concentrated dye solutions change color so slowly, any oxidized ITS will be converted back to reduced ITS due to high concentrations of bisulfite in the inner ITS environment. This observation also supports the hypothesis that the behavior seen in the kinetics of the short time data is influenced by the release of bisulfite from the inner environment as the temperature is increased. A high concentration of bisulfite in the inner environment at the 1:10 dilution would influence the observed rates of reaction for the short time kinetics as more energy is put into the system and a higher fraction of bisulfite occupies the outer environment.

While the higher temperature kinetic data of the 1:10 dye solutions does show the expected decrease in the fluorescence signal, the rate of fluorescence decrease is still likely to be a combination of both the forward reaction, $ITS_{red} \rightarrow ITS_{ox}$, and the reverse reaction, $ITS_{ox} \rightarrow ITS_{red}$. However, second derivative analysis of the long time kinetic data of the 1:10 dilutions of the dye solutions show a distinct inflection in the latter half of the experiment that corresponds to an increase in the forward rate, $ITS_{red} \rightarrow ITS_{ox}$, that is likely due reverse reaction becoming less significant. Modeling the rate of reaction at this accelerated long time rate would therefore yield the best estimate of the reaction rate for temperatures above 40 °C. The forward reaction rates at 30 and 40 °C for the 1:10 dilution can be estimated from equation 7 by plotting ln(k/T) vs 1/T for the rates at 50, 60, and 70 °C and using the best fit slope and intercept to calculate the forward rate of reaction at 30 and 40 °C. Kinetic experiments with dilutions greater than 1:10 show no evidence of the back reaction occurring. While some back reaction cannot be ruled out the data shows that the forward reaction, $ITS_{red} \rightarrow ITS_{ox}$, dominates for solutions with a greater than 1:10 dilution.

Tables 9, 10 and 11 show the first order rate constants for dye solution 1, 2, and 3 for all dilutions over the temperature range from 30 to 70 °C. The percent relative

 http://dx.doi.org/10.1016/j.heliyon.2017.e00397

Table 9. Long time kinetic data for ink solution 1. R^2 values are the square of the correlation coefficient for the fit of the kinetic data to the first order model. Data marked with an * represent estimated rates as described in the manuscript.

Temperature °C	First Order Rate Constant for 1 to 10 Dilution (s^{-1})	First Order Rate Constant for 1 to 100 Dilution (s^{-1})	First Order Rate Constant for 1 to 500 Dilution (s^{-1})	First Order Rate Constant for 1 to 1000 Dilution (s^{-1})
30	$1.1 \times 10^{-5*}$	1.4×10^{-5} $R^2 = 0.952$	9.7×10^{-6} $R^2 = 0.922$	1.7×10^{-5} $R^2 = 0.967$
40	$3.5 \times 10^{-5*}$	1.4×10^{-5} $R^2 = 0.994$	1.5×10^{-5} $R^2 = 0.959$	2.7×10^{-5} $R^2 = 0.967$
50	1.0×10^{-4} $R^2 = 0.997$	7.3×10^{-5} $R^2 = 0.988$	4.1×10^{-5} $R^2 = 0.982$	6.4×10^{-5} $R^2 = 0.979$
60	3.0×10^{-4} $R^2 = 0.995$	2.4×10^{-4} $R^2 = 0.966$	1.9×10^{-4} $R^2 = 0.957$	3.4×10^{-4} $R^2 = 0.982$
70	7.0×10^{-4} $R^2 = 0.996$	5.7×10^{-4} $R^2 = 0.979$	3.8×10^{-4} $R^2 = 0.989$	6.2×10^{-4} $R^2 = 0.966$

standard deviation in the first order rate constants for dye solution 1 and 3 across the dilutions is 28 and 26 percent respectively. First order rate constants for dye solution 2 across all dilutions display a relative standard deviation of three times larger than dye solutions 1 and 3, 77 percent. This indicates the lower concentration of PDADMAC in dye solution 2 does not yield a PEC that is as stable with dilution as the dye solutions with higher PDADMAC concentrations. The similarity in the relative standard deviation of the rate data for dye solutions 1 and 3 indicate that increasing the PDADMAC concentration beyond 3.2×10^{-4} M PDADMAC (monomer unit concentration) does not result in a PEC that is significantly more stable with dilution.

Tables 12, 13 and 14 give $\Delta^{\ddagger}H$ and $\Delta^{\ddagger}S$ values calculated from the kinetic data for dye solutions 1, 2, and 3. As discussed previously, the more dilute samples are likely to have the smallest back reaction, $ITS_{ox} \rightarrow ITS_{red,}$ contribution to the kinetic data. The data in Tables 12, 13 and 14 show that $\Delta^{\ddagger}H$ is very consistent for all three dye solutions across the 1:100 to the 1:1000 dilutions. All three ink solutions have $\Delta^{\ddagger}H$ values that are identical within the uncertainties for dilutions ranging

Table 10. Long time kinetic data for dye solution 2. R^2 values are the square of the correlation coefficient for the fit of the kinetic data to the first order model. Data marked with an * represent estimated rates as described in the manuscript.

Temperature °C	First Order Rate Constant for 1 to 10 Dilution (s^{-1})	First Order Rate Constant for 1 to 100 Dilution (s^{-1})	First Order Rate Constant for 1 to 500 Dilution (s^{-1})	First Order Rate Constant for 1 to 1000 Dilution (s^{-1})
30	$4.6 \times 10^{-6*}$	8.4×10^{-6} $R^2 = 0.835$	2.6×10^{-5} $R^2 = 0.984$	9.2×10^{-5} $R^2 = 0.994$
40	$2.6 \times 10^{-5*}$	1.5×10^{-5} $R^2 = 0.987$	4.7×10^{-5} $R^2 = 0.992$	5.4×10^{-5} $R^2 = 0.990$
50	9.5×10^{-5} $R^2 = 0.949$	3.7×10^{-5} $R^2 = 0.989$	1.6×10^{-4} $R^2 = 0.982$	3.3×10^{-4} $R^2 = 0.956$
60	8.5×10^{-4} $R^2 = 0.996$	1.6×10^{-4} $R^2 = 0.981$	5.2×10^{-4} $R^2 = 0.981$	1.2×10^{-3} $R^2 = 0.959$
70	1.6×10^{-3} $R^2 = 0.994$	8.5×10^{-4} $R^2 = 0.960$	2.7×10^{-3} $R^2 = 0.980$	3.6×10^{-3} $R^2 = 0.992$

http://dx.doi.org/10.1016/j.heliyon.2017.e00397

Table 11. Long time kinetic data for dye solution 3. R^2 values are the square of the correlation coefficient for the fit of the kinetic data to the first order model. Data marked with an * represent estimated rates as described in the manuscript.

Temperature °C	First Order Rate Constant for 1 to 10 Dilution (s^{-1})	First Order Rate Constant for 1 to 100 Dilution (s^{-1})	First Order Rate Constant for 1 to 500 Dilution (s^{-1})	First Order Rate Constant for 1 to 1000 Dilution (s^{-1})
30	$3.6 \times 10^{-7*}$	1.2×10^{-5} $R^2 = 0.950$	2.2×10^{-5} $R^2 = 0.963$	1.7×10^{-5} $R^2 = 0.941$
40	$1.9 \times 10^{-6*}$	2.5×10^{-5} $R^2 = 0.994$	2.3×10^{-5} $R^2 = 0.973$	2.5×10^{-5} $R^2 = 0.964$
50	1.0×10^{-5} $R^2 = 0.971$	4.5×10^{-5} $R^2 = 0.994$	6.6×10^{-5} $R^2 = 0.986$	5.7×10^{-5} $R^2 = 0.980$
60	3.7×10^{-5} $R^2 = 0.995$	1.5×10^{-4} $R^2 = 0.979$	4.0×10^{-4} $R^2 = 0.989$	3.1×10^{-4} $R^2 = 0.953$
70	8.1×10^{-5} $R^2 = 0.991$	5.8×10^{-4} $R^2 = 0.956$	1.0×10^{-3} $R^2 = 0.959$	3.6×10^{-4} $R^2 = 0.949$

from 1:100 to 1:1000. This consistency for a given dilution indicates that neglection of the reverse reaction is reasonable for solutions at dilutions of 1:100 to 1:1000. This indicates that energetics of the activated complex are essentially equivalent for the three dye solutions despite the PDADMAC concentration changing by a factor of ~3 between the different solutions and the individual solution concentration changing by 2 orders of magnitude. Within the uncertainties the $\Delta^{\ddagger}H$ for dye solutions 1 and 2 at a 1:10 dilution are indistinguishable from the $\Delta^{\ddagger}H$ of the dilutions of the respective solutions. The 1:10 dilution of dye solution 3, however, displays a statistically significantly increased $\Delta^{\ddagger}H$ relative to the diluted dye 3 solutions. This increased $\Delta^{\ddagger}H$ indicates that within the inner environment the greater concentration of PDADMAC in dye solution 3 makes oxidation of the ITS more difficult. Even if the larger $\Delta^{\ddagger}H$ of dye solution 3 is influenced by the back reaction of the $ITS_{ox} \rightarrow ITS_{red}$ in the inner PEC environment the magnitude of $\Delta^{\ddagger}H$ shows the increased barrier to the rate of ITS oxidation.

Due to the nature of the analysis using equation 7, significant error exists in the calculation of $\Delta^{\ddagger}S$ for the slower reaction rates of the inner environment but Tables 11, 12 and 13 do show that the $\Delta^{\ddagger}S$ to be consistently in the range of −20 to −80 J/molK. Dye solution 2 does show a positive $\Delta^{\ddagger}S$ for the 1:10 dilution, 74 ±

Table 12. Activation parameters for dye solution 1.

Dilution for dye solution 1	$\Delta^{\ddagger}H$ (kJ/mol)	$\Delta^{\ddagger}S$ (J/molK)
1 to 10 Dilution	87 ± 5	–53 ± 15
1 to 100 Dilution	95 ± 14	–28 ± 18
1 to 500 Dilution	85 ± 9	–16 ± 30
1 to 1000 Dilution	81 ± 10	–71 ± 32

http://dx.doi.org/10.1016/j.heliyon.2017.e00397

Table 13. Activation parameters for dye solution 2.

Dilution for dye solution 2	$\Delta^{\ddagger}H$ (kJ/mol)	$\Delta^{\ddagger}S$ (J/molK)
1 to 10 Dilution	128 ± 40	74 ± 120
1 to 100 Dilution	93 ± 15	–37 ± 47
1 to 500 Dilution	98 ± 11	–12 ± 33
1 to 1000 Dilution	87 ± 23	–43 ± 60

120 J/molK, but given the large uncertainty in the value it is unlikely that the positive $\Delta^{\ddagger}S$ is a valid value.

The average $\Delta^{\ddagger}H$ value for the long time kinetics is greater by a factor of 2.3 and the $\Delta^{\ddagger}S$ is reduced by a factor 3.2 relative to the short time data. The inner PEC environment requires significantly more energy to drive the oxidation of ITS_{red} as expected. Additionally, the activated complex in the inner environment is much closer in structure to the ground state reactants than the activated complex for the outer environment. This is result is expected since the inner complex is a more closed structure and would have a higher degree of order than the outer complex.

Tables 15 and 16 show the kinetic data for dye solutions 4 and 5 which respectively contain half the amount of sodium bisulfite as inks 1–3 and 50% more of the sodium bisulfite than dye solutions 1–3. Tables 17 and 18 show the $\Delta^{\ddagger}H$ and $\Delta^{\ddagger}S$ values for dye solutions 4 and 5. Activation enthalpy and entropy values for dye solution 4 are similar to what is seen for dye solution 1 and 2 and dilutions of dye solution 3 greater than 1:10. Dye solution 5 at a 1:10 dilution has a significantly lower enthalpy of activation, 39 ± 9 kJ/mol, and a significantly higher $\Delta^{\ddagger}S$, −189 ± 24 J/molK, than the 1:10 dilutions of dye solutions 1–3. The values of the $\Delta^{\ddagger}H$ and $\Delta^{\ddagger}S$ for the 1:10 dilution of dye solution 5 are statistically indistinguishable from the activation parameters of the outer PEC environment. This indicates that the inner PEC for dye solution 5 at the 1 to 10 dilution is quite open. The higher ionic strength of dye solution 5 can provide more charge shielding of the polyelectrolyte complex and therefore the interactions between ITS and PDADMAC are not as strong in the inner environment. This would lead to an inner PEC that is less protective of the ITS_{red} and result in a lower energy barrier to

Table 14. Activation parameters for dye solution 3.

Dilution for dye solution 3	$\Delta^{\ddagger}H$ (kJ/mol)	$\Delta^{\ddagger}S$ (J/molK)
1 to 10 Dilution	131 ± 19	–69 ± 39
1 to 100 Dilution	80 ± 10	–78 ± 30
1 to 500 Dilution	87 ± 16	–53 ± 48
1 to 1000 Dilution	91 ± 14	–41 ± 42

http://dx.doi.org/10.1016/j.heliyon.2017.e00397

Table 15. Long time kinetic data for dye solution 4. R^2 values are the square of the correlation coefficient for the fit of the kinetic data to the first order model. Data marked with an * represent estimated rates as described in the manuscript.

Temperature °C	First Order Rate Constant for 1 to 10 Dilution (s^{-1})	First Order Rate Constant for 1 to 100 Dilution (s^{-1})
30	$3.1 \times 10^{-8*}$	2.6×10^{-5} $R^2 = 0.891$
40	$6.3 \times 10^{-7*}$	1.6×10^{-5} $R^2 = 0.989$
50	8.1×10^{-6} $R^2 = 0.812$	2.8×10^{-5} $R^2 = 0.997$
60	2.8×10^{-4} $R^2 = 0.997$	1.0×10^{-4} $R^2 = 0.986$
70	1.4×10^{-3} $R^2 = 0.997$	4.6×10^{-4} $R^2 = 0.986$

ITS oxidation. Even at a 1:10 dilution for dye solution 5 the inner environment of the PEC remains more open than the PECs in other solutions.

The inner environment of dye solution 5 still contains a significant amount of bisulfite, partitioning data shows the fraction of ITS_{red} in the outer environment is 0.10 at 30 °C and the bisulfite is assumed to be similar. With increasing temperature, more bisulfite is present in the outer environment creating a higher local concentration of bisulfite in the outer environment. This leads to stagnant or decreasing reaction rates seen in the kinetic data for the outer environment of this dye solution. Less bisulfite in the inner environment would lead to a less open inner structure due to decreased electrostatic shielding between bisulfite and PDADMAC monomer units.

Tables 19 and 20 show the first order fits of the 1:10 dilution of dye solutions 3 and 5 in 500 mM NaCl. Activation enthalpies for dye solution 3 and 5 with 500 mM NaCl added are shown in Table 21. The increased ionic strength for ink 3 reduces the $\Delta^{\ddagger}H$ value by a factor of 2.1, 143 ± 9 kJ/mol with no salt added and 68 ± 19 kJ/mol with salt added. This result provides supporting evidence that the ionic

Table 16. Long time kinetic data for dye solution 5. R^2 values are the square of the correlation coefficient for the fit of the kinetic data to the first order model. Data marked with an * represent estimated rates as described in the manuscript.

Temperature °C	First Order Rate Constant for 1 to 10 Dilution (s^{-1})	First Order Rate Constant for 1 to 100 Dilution (s^{-1})
30	$2.5 \times 10^{-5*}$	1.4×10^{-5} $R^2 = 0.813$
40	$4.3 \times 10^{-5*}$	2.4×10^{-5} $R^2 = 0.996$
50	6.7×10^{-5} $R^2 = 0.995$	3.7×10^{-5} $R^2 = 0.995$
60	1.2×10^{-4} $R^2 = 0.995$	2.3×10^{-4} $R^2 = 0.969$
70	1.6×10^{-4} $R^2 = 0.997$	7.7×10^{-4} $R^2 = 0.970$

http://dx.doi.org/10.1016/j.heliyon.2017.e00397

Table 17. Activation parameters for dye solution 4.

Dilution for dye solution 4	$\Delta^{\ddagger}H$ (kJ/mol)	$\Delta^{\ddagger}S$ (J/molK)
1 to 10 Dilution	89 ± 17	–43 ± 35
1 to 100 Dilution	98 ± 16	–26 ± 48

strength of the solution effects the ability of the inner environment to encapsulate the ITS_{red} and shield ITS_{red} from oxidation even with the higher concentration of PDADMAC in dye solution 3. Results for dye solution 5 (50% more sodium bisulfite added) show that there is an upper limit of the ionic strength effect as the addition of NaCl showed no statistically significant difference in the activation enthalpies, 39 ± 9 kJ/mol with no NaCl added and 44 ± 6 kJ/mol with NaCl added (the activation entropies were also identical within the uncertainties, −189 ± 24 J/molK with no NaCl added and −180 ± 18 J/molK with salt added). This result for the 1:10 dilution dye solution 5 is consistent with the results discussed above for no NaCl added to the 1:10 dilution of dye solution 5.

Dye solution 5 at a 1:10 dilution with and without NaCl added has an activation enthalpy for the inner PEC environment that is statistical indistinguishable from the activation enthalpy of the outer PEC environment. However, the entropies of activation for the inner environment of both 1:10 dilutions of dye 5 solutions are a factor of 6 greater than what is observed on average for inner PEC environments of dye solutions 1–3. The values of the entropies of activation are also greater than the average entropy of activation for the outer PEC environment, −189 J/molK and −180 J/molK for the 1:10 dilutions of dye solution 5 with and without salt added respectively and −130 J/molK for the average entropy of activation of the outer PEC environment. Even though the activation enthalpies are similar the rates of the oxidation of the ITS_{red} in the inner environment of dye solutions 5 at a 1:10 dilution do not correspond to the rates of oxidation in the outer environment due to the increased entropy of the activated complex.

Activation enthalpies for dye solutions 4 and 5 at a 1:100 dilution show values that are similar to dye solutions 1–3 at the 1:100 dilutions (see Tables 19 and 20). Consistency of the activation parameters indicates that the structure of the polyelectrolyte complex is reasonably similar across the all dye solutions at dilutions of 1:100. This result is reasonable since the ionic strengths of all inks will

Table 18. Activation parameters for dye solution 5.

Dilution for dye solution 5	$\Delta^{\ddagger}H$ (kJ/mol)	$\Delta^{\ddagger}S$ (J/molK)
1 to 10 Dilution	39 ± 9	–189 ± 24
1 to 100 Dilution	106 ± 18	2 ± 57

http://dx.doi.org/10.1016/j.heliyon.2017.e00397

Table 19. Long time kinetic data for dye solution 3 in 500 mM NaCl. R^2 values are the square of the correlation coefficient for the fit of the kinetic data to the first order model. Data marked with an * represent estimated rates as described in the manuscript.

Temperature °C	First Order Rate Constant for 1 to 10 Dilution (s^{-1})
30	$4.2 \times 10^{-5*}$
40	$1.0 \times 10^{-4*}$
50	2.1×10^{-4} $R^2 = 0.992$
60	6.6×10^{-4} $R^2 = 0.991$
70	9.6×10^{-4} $R^2 = 0.996$

be low at the 1:100 dilutions and have a much smaller effect on the kinetic data. The increase in the $\Delta^{\ddagger}H$ by a factor of over 2 and the change in $\Delta^{\ddagger}S$ from −189 to near 0 J/molK for dye solution 5 at the 1:100 dilutions relative to the 1:10 dilution indicates that there is a significant rearrangement in the structure of the inner PEC with dilution. This rearrangement is likely due to HSO_3^- leaving the inner PEC and resulting in a more closed and protective inner PEC due to less electrostatic shielding. This result suggests that the concentration of the HSO_3^- in the inner PEC is not as important as the structure of the inner PEC in reducing the rate of ITS_{red} oxidation.

The long time kinetic data shows that the second kinetic component persists in the dye regardless of the dilutions, concentration ranges of PDADMAC, temperatures, ionic strength, and concentration ranges of bisulfite studied. This suggests the polyelectrolyte encapsulation of ITS_{red} forms a relatively stable complex in the initial dye solution and is not easily disrupted by the changes in the solution phase environment included in this study. Increasing the ionic strength of the dye solution can disrupt the inner environment of the complex and results in a lower activation

Table 20. Long time kinetic data for dye solution 5 in 500 mM NaCl. R^2 values are the square of the correlation coefficient for the fit of the kinetic data to the first order model. Data marked with an * represent estimated rates as described in the manuscript.

Temperature °C	First Order Rate Constant for 1 to 10 Dilution (s^{-1})
30	$5.6 \times 10^{-5*}$
40	$1.0 \times 10^{-4*}$
50	1.9×10^{-4} $R^2 = 0.971$
60	2.8×10^{-4} $R^2 = 0.963$
70	5.2×10^{-4} $R^2 = 0.908$

http://dx.doi.org/10.1016/j.heliyon.2017.e00397

Table 21. Activation parameters for dye solution 3 and 5 in the presence of 500 mM NaCl.

	$\Delta^{\ddagger}H$ (kJ/mol)	$\Delta^{\ddagger}S$ (J/molK)
Dye Solution 3 with NaCl 1 to 10 Dilution	68 ± 19	–105 ± 58
Dye Solution 5 with NaCl 1 to 10 Dilution	44 ± 6	–180 ± 18

barrier and a more rapid oxidation of the ITS_{red}. Diluted dye solutions that are prepared in higher ionic strength are not significantly affected by addition of NaCl.

Assuming that the dye solutions are at or very near equilibrium in terms of the number of ITS_{red} molecules in the outer and inner environments of the PEC at the beginning of the fluorescence experiments, an estimate of the partition function, K, can be made from the fluorescence data using the following equation:

$$K = \frac{[ITS_{red}]^{\circ}_{outer}}{[ITS_{red}]^{\circ}_{inner}} \quad (8)$$

Where K is the partition coefficient, $[ITS_{red}]^{\circ}_{outer}$ is the initial concentration of the ITS_{red} in the outer environment estimated from the kinetic data, and $[ITS_{red}]^{\circ}_{inner}$ is the concentration of the inner environment estimated from the kinetic data (see equation 6). Using the partitioning coefficient from equation 8, estimates of the enthalpy and entropy of the partitioning can be calculated by rearrangement of the well-known Gibbs free energy equations

$$\Delta G^{\circ}_{partitioning} = \Delta H^{\circ}_{partitioning} - T\ \Delta S^{\circ}_{partitioning} \quad (9)$$

$$\Delta G^{\circ}_{partitioning} = -RTln(K) \quad (10)$$

to yield:

$$In(K) = \frac{-\Delta H^{\circ}_{partitioning}}{RT} + \frac{\Delta S^{\circ}_{partitioning}}{R} \quad (11)$$

Where K is the partition coefficient, T is the temperature of the system in kelvin, R is the ideal gas constant of 8.314 J/molK, $\Delta G^{\circ}_{partitioning}$ is the standard Gibbs free energy of partitioning, $\Delta H^{\circ}_{partitioning}$ is the standard enthalpy of partitioning, and

Table 22. Thermodynamic partitioning parameters for dye solution 1.

Dilution for dye solution 1	ΔH (kJ/mol)	ΔS (J/molK)
1 to 10 Dilution	54 ± 9	171 ± 28
1 to 100 Dilution	58 ± 6	176 ± 18
1 to 500 Dilution	71 ± 6	220 ± 17
1 to 1000 Dilution	73 ± 4	225 ± 13

http://dx.doi.org/10.1016/j.heliyon.2017.e00397

Table 23. Thermodynamic partitioning parameters for dye solution 2.

Dilution for dye solution 2	ΔH (kJ/mol)	ΔS (J/molK)
1 to 10 Dilution	80 ± 13	236 ± 41
1 to 100 Dilution	59 ± 6	179 ± 17
1 to 500 Dilution	59 ± 1	177 ± 4
1 to 1000 Dilution	60 ± 9	186 ± 29

$\Delta S^{\circ}_{partitioning}$ is the standard entropy of partitioning. Plotting 1/T versus ln(K) allows $\Delta H^{\circ}_{partitioning}$ and $\Delta S^{\circ}_{partitioning}$ to be calculated using equation 11.

Calculation of the partitioning coefficient from equation 8 yields the fraction of ITS_{red} molecules in the inner and outer environments. The 1:10 dilutions of ink solutions 1, 2, and 3 show the fraction of ITS_{red} molecules in the outer environment to be 0.07 ± .03 at 30 °C and 0.48 ± 0.04 at 70 °C. The fraction of ITS_{red} molecules in the outer environment at 30 °C is similar for dye solutions 4 and 5 as well as dye solutions 3 and 5 with 500 mM NaCl. However, dye solutions 3 and 5 with 500 mM NaCl added show a significant increase with temperature in the fraction of ITS_{red} molecules in the outer environment, 0.76 ± 0.04 and 0.87 ± .07 at 70 °C for dye solutions 3 and 5 respectively. The above data show that the increased ionic strength does not significantly alter the partitioning of the ITS_{red} molecules at 30 °C but as energy is added to the system the increased ionic strength disrupts the macromolecular complex. This leads to a significantly higher fraction of the ITS_{red} molecules existing in the outer environment. This higher fraction of molecules in the outer environment leads to the counter intuitive kinetic behavior discussed for the short time kinetics of the dye solutions.

Dilution of the dye solution does lead to a more open PDADMAC/ITS_{red} complex as the temperature is increased. Average ITS_{red} fractions in the outer environment across all dye solutions of 1:100 at 30 °C are similar to those seen for the 1:10 dilutions, 0.07 ± .03 and 0.09 ± .03 for the 1:10 and 1:100 dilution respectively. At 70 °C the average fraction of ITS_{red} in the outer environment is 0.71 ± 0.07 for the 1:100 dye dilutions which is 48% greater than what is measured for the 1:10 dilutions. Dilution of dye solutions of 1:1000 show a greater average fraction of

Table 24. Thermodynamic partitioning parameters for dye solution 3.

Dilution for dye solution 3	ΔH (kJ/mol)	ΔS (J/molK)
1 to 10 Dilution	61 ± 2	183 ± 6
1 to 100 Dilution	87 ± 12	269 ± 38
1 to 500 Dilution	69 ± 4	211 ± 13
1 to 1000 Dilution	60 ± 9	235 ± 35

http://dx.doi.org/10.1016/j.heliyon.2017.e00397

Table 25. Thermodynamic partitioning parameters for dye solution 4.

Dilution for dye solution 4	ΔH (kJ/mol)	ΔS (J/molK)
1 to 10 Dilution	89 ± 8	265 ± 30
1 to 100 Dilution	63 ± 9	192 ± 28

ITS_{red} in the outer environment at 30 °C than the 1:10 or 1:100 dilutions, 0.18 ± 0.09. At 70 °C the 1:1000 dilutions show largest fraction of ITS_{red} in the outer environment, 0.83 ± 0.04, which is equivalent within the uncertainties to what is seen with 1:10 dilution of dye solutions with 500 mM NaCl added. This data does indicate that dilution of the dye solutions and addition of heat can open up the structure of the PDADMAC/ITS_{red} complex but a significant majority of the ITS_{red} still exists in the inner complex at moderate temperatures.

Tables 20, 21, 22, 23, 24, 25, 26 and 27 show the $\Delta H^{\circ}_{partitioning}$ and $\Delta S^{\circ}_{partitioning}$ calculated using equation 7. Partitioning to the inner environment is enthalpically favored with enthalpies ranging from 54 to 89 kJ/mol. Partitioning to the outer environment is entropically favored with entropies ranging from 171 to 270 J/molK. The ΔG° for the partitioning at 30 °C favors the partitioning of the ITS into the inner complex. The mechanism of the increase in the number ITS_{red} in the outer environment of the PEC is likely due to the PEC structure becoming more open as the temperature is increased. This would increase the number of binding sites between the ITS and the PDADMAC in the more open, less protective, outer type environment.

With addition of NaCl to dye solutions 3 and 5, 1:10 dilution, the enthalpy of partitioning increases for both solutions, 77 ± 4 kJmol with NaCl added compared to 61 ± 2 kJ/mol without NaCl for dye solution 3 and 93 ± 7 kJ/mol with NaCl added compared to 60 ± 12 kJ/mol without NaCl added for dye solution 5. However, the entropy of partitioning also increases, 236 ± 14 J/molK with NaCl added compared to 183± 6 J/molK without NaCl for dye solution 3 and 286 ± 21 J/molK with NaCl added compared to 178 ± 38 J/molK without NaCl added for dye solution 5. Increase in the entropy of both solutions with NaCl added is expected as more ions would be released to solution with an increase in temperature. Increased partitioning to the outer environment with addition of NaCl ultimately increases the rate of the observed oxidation of the ITS. Even if the outer PEC environment

Table 26. Thermodynamic partitioning parameters for dye solution 5.

Dilution for dye solution 5	ΔH (kJ/mol)	ΔS (J/molK)
1 to 10 Dilution	60 ± 12	178 ± 37
1 to 100 Dilution	67 ± 10	204 ± 31

http://dx.doi.org/10.1016/j.heliyon.2017.e00397

Table 27. Thermodynamic partitioning parameters for dye solution 3 and 5 in the presence of 500 mM NaCl.

	ΔH (kJ/mol)	ΔS (J/molK)
Dye Solution 3 with NaCl 1 to 10 Dilution	77 ± 4	236 ± 14
Dye Solution 5 with NaCl 1 to 10 Dilution	93 ± 7	286 ± 21

becomes less open as is the case with NaCl added for dye solution 5, the oxidation rate of ITS is still increased in the outer PEC environment relative to the inner PEC environment.

4. Conclusion

Preparation of dye solutions with ITS_{red} and PDADMAC as outlined in this manuscript result in PECs that are stable from room temperature to 70 °C and at dilutions ranging from 1:10 to 1:1000. These PEC complexes stabilize the ITS_{red} and inhibit the oxidation of the ITS_{red} molecule in atmospheric environments. Spectroscopic analysis of the dye solutions show that the ITS_{red} exists in the PEC in an aggregated complex and the concentration of the ITS monomer is not significant under the experimental conditions. Kinetic studies using fluorescence spectroscopy with excitation of the aggregation band at 520 nm show that two distinct kinetic regimes exist for the oxidation of ITS_{red}. These two distinct kinetic domains are likely due to ITS_{red} aggregation in an outer PEC environment leading to relatively rapid oxidation of ITS_{red} and ITS_{red} aggregation in an inner PEC environment leading to slower oxidation of the ITS_{red}. Analysis of the oxidation of the ITS_{red} in PEC environments using Eyring transition state theory shows that the $\Delta^{\ddagger}H$ is very similar for dye solutions 1 through 3 at dilutions ranging from 1:100 to 1:1000. This indicates that the mechanism for the oxidation of the ITS_{red} is similar for the PEC formed in all three solutions at these dilutions despite the PDADMAC concentration varying by a factor of 3. The $\Delta^{\ddagger}H$ for dye solution 3 at a 1:10 dilution is greater than the $\Delta^{\ddagger}H$ for dye solution 1 at a 1:10 dilution with statistical significance. This is likely due to the greater concentration of the PDADMAC in dye solution 3 and greater stabilization of the inner PEC complex in this solution. Dye solution 3 does display a significant decrease in the $\Delta^{\ddagger}H$ when the 1:10 dilution is prepared in 100 mM NaCl indicating that the increased ionic strength forces a more open inner PEC that is not as protective of the ITS_{red}.

Analysis of the kinetic data of the inner PEC when the concentration of bisulfite is reduced by 50% for dye solution 1 yields a $\Delta^{\ddagger}H$ that is similar to the original dye solution. However, increasing the bisulfite concentration of dye solution 1 by 50% yields a statistically significant reduction in the $\Delta^{\ddagger}H$ for the solution at a 1:10 dilution indicating the higher ionic strength of the initial dye solution results in a

http://dx.doi.org/10.1016/j.heliyon.2017.e00397

more open PEC complex. The presence of 500 mM NaCl at a 1:10 dilution yields little change in $\Delta^{\ddagger}H$ for the solution with 50% higher bisulfite concentration indicating that the PEC is not significantly disrupted by the addition of NaCl.

Use of the fluorescence data to estimate the partitioning of ITS_{red} molecules between the inner and outer PEC shows that the partitioning to the outer PEC is entropically driven. While the data is modeled as a partitioning coefficient the mechanism suggested by the data governing the increase of the ITS_{red} in the outer PEC is by the PEC becoming more open as the temperature is increased, this provides a larger concentration of binding sites in an outer type environment for the ITS_{red} to interact with.

Declarations

Author contribution statement

Becca Hoene: Conceived and designed the experiments; Performed the experiments; Analyzed and interpreted the data; Wrote the paper.

Dion Rivera: Conceived and designed the experiments; Performed the experiments; Analyzed and interpreted the data; Contributed reagents, materials, analysis tools or data; Wrote the paper.

Funding statement

Professor Dion Rivera received funding from Sensor International, LLC. (formerly Sensor, LLC.) during the early stages of this work. Becca Hoene received summer salary funding from the School of Graduate Studies and Research at Central Washington University.

Competing interest statement

The authors declare the following conflict of interests: Dion Rivera; [Professor Dion Rivera received funding from Sensor International, LLC. (formerly Sensor, LLC.) during the early stages of this work. This company included professor Rivera as a co-inventor on the patents related to ink systems that incorporate the chemistry described in the manuscript. The patents are wholly owned by the company and professor Rivera does not receive any royalties related to the patents. Professor Rivera has not received any financial compensation from Sensor International, LLC. since 2015. Supplies and equipment provided by Sensor International, LLC. were used in the research described in the manuscript].

Additional information

No additional information is available for this paper.

http://dx.doi.org/10.1016/j.heliyon.2017.e00397

Acknowledgements

Mr. David Bryce is acknowledged for early contributions to the work is this manuscript. Mr. Caleb Kaiser is acknowledged for obtaining the data used in Figs. 3, 4, and 6.

References

[1] G. Heacock, D. Rivera, Color changeable dyes for indicating exposure, methods of making and using such dyes and apparatuses incorporating such dyes, U.S. Patent 8663998 (2014) March 4.

[2] G. Heacock, D. Rivera, Color changeable dyes for indicating exposure, methods of making and using such dyes and apparatuses incorporating such dyes, U.S. Patent 9486591 (2016) November 8.

[3] A. Mills, N. Wills, Reductive Photocatalyists and Smart Inks, Chem. Soc. Rev. 44 (2015) 2849–2864.

[4] S.-K. Lee, M. Sheridan, A. Mills, Novel UV-Activated Colorimetric Oxygen Indicator, Chem. Mater. 17 (2005) 2744–2751.

[5] A. Mills, C. Tommons, R.T. Bailey, M.C. Tedford, P.J. Crilly, UV-Activated Luminesence/Colourmetric O_2 Indicator, Int. J. Photoenergy (2008).

[6] A. Mills, Q. Chang, N. McCurray, Equilibrium Studies on Colorimetric Plastic Film Sensors for Carbon Dioxide, Anal. Chem. 64 (1992) 1383–1389.

[7] M. Imran, A.B. Yousaf, X. Zhou, K. Liang, Y.-F. Jiang, A.-X. Xu, Oxygen-Deficient TiO_{2-x}/Methylene Blue Colloids: Highly Efficient Photoreversible Ink, Langmuir 32 (2016) 8980–8987.

[8] A. Mills, D. Hazafi, Nanocrystalline SnO_2-based, UV-activated, Colourimetric Oxygen Indicator, Sens. Actuators B 136 (2009) 344–349.

[9] Y. Galagan, W.F. Su, Reversible Photoreduction of Methylene Blue in Acrylate Media Containing Benzyl Dimethyl Ketal, J. Photochem. Photobiol. A 195 (2008) 378–383.

[10] D.W. Miller, J.G. Wilkes, E.D. Conte, Food quality indicator device, U.S. Patent 7 (014) (2006) 816.

[11] C. Bultzingslowen, A.K. McEvoy, C. McDonagh, B.D. MacCraith, I. Klimant, C. Krause, O.S. Wolfbeis, Sol-gel based optical carbon dioxide sensor employing dual luminophore referencing for application in food packaging technology, Analyst 127 (2002) 1478–1483.

 http://dx.doi.org/10.1016/j.heliyon.2017.e00397

[12] I. Gill, Bio-doped nanocomposite polymers: Sol-gel bioencapsulates, Chem. Mater. 13 (2001) 3404–3421.

[13] A. Mills, Oxygen Indicators in Food Packaging, In: M.I. Baraton (Ed.), Sensors for Environment, Health, and Security, Springer Science, 2009.

[14] A. Mills, Oxygen Indicators and Intelligent Inks for Food Packaging, Chem. Soc. Rev. 34 (2005) 1003–1011.

[15] A. Mills, S.K. Lee, Sensor for Oxidizing Agents Patent WO 03/021252, Strathclyde University, 2003, 2017.

[16] D.L. Putnam, T. Hubbard, Process for Forming Polymer Structures Containing an Oxygen Sensor, U.S. Patent 6 (794) (2004) 191.

[17] E.W. Saaski, D.A. McCrae, D.M. Lawrence, Metri Optical Oxygen Sensor Cor. Inc, U.S. Patent 5 (039) (1991) 491.

[18] M.R. Shahriari, Patches for non-intrusive monitoring of oxygen in packages, U.S. Patent 7 (862) (2011) 770.

[19] T.A. Blinka, C. Bull, C.R. Barmor, D.V. Speer, Co. Grace, Method of Detecting the Permeability of an Object to Oxygen, U.S. Patent 5 (583) (1996) 047.

[20] Polymer Surfactant Systems, In: J.C.T. Kwak (Ed.), Surfactant Science Series, 77, Marcel Dekker, New York, 1998.

[21] Y. Wang, J. Banziger, P.L. Dubin, G. Filippelli, N. Nuraje, Adsorptive Partitioning of an Organic Compound onto Polyelectrolyte-Immobilized Micelles on Porous Glass and Sand, Environ. Sci. Technol. 35 (2001) 2608–2611.

[22] Y.G. Mishael, P.L. Dubin, Uptake of Organic Pollutants by Silica-Polycation-Immobilized Micelles for Groundwater Remediation, Environ. sci. Technol. 39 (2005) 8475–8480.

[23] Q. Jai, C. Song, H. Li, Z. Zhang, H. Liu, Y. Yu, T. Wang, Synthesis of strongly cationic hydrophobic polyquaternium flocculants to enhance removal of water-soluble dyes in wastewater, Res. Chem. Intermediat. 43 (5) (2017) 3395–3413.

[24] I.A. Shabtai, Y.G. Mishael, Efficient Filtration of Effluent Organic Matter by Polycation-Clay Composite Sorbents: Effect of Polycation Configuration on Pharmaceutical Removal, Environ. Sci. Technol. 50 (2016) 8246–8254.

 http://dx.doi.org/10.1016/j.heliyon.2017.e00397

[25] D.O. Grigoriev, K. Kohler, E. Skorb, D.G. Shchukin, H. Mohwald, Polyelectrolyte Complexes as a 'Smart' Depot for Self-Healing Anticorrosion, Soft Matter 5 (2009) 1426–1432.

[26] M.L. Zheludkevich, J. Tedim, M.G.S. Ferreira, Smart coatings for active corrosion prevention based on multifunctional micro and nanocontainers, Electrochim. Acta 82 (2012) 314–323.

[27] X. Shi, M. Shem, H. Möhwald, Polyelectrolyte multilayer nanoreactors toward the synthesis of diverse nanostructured materials, Prog. Polym. Sci. 29 (2004) 987–1019.

[28] R. Ghan, T. Shutava, A. Patel, V.T. John, Y. Lvov, Enzyme-Catalized polymerization of phenols within polyelectrolyte microcapsules, Macromolecules 37 (2004) 4519–4524.

[29] Y. Zhu, K. Chen, X. Wang, X. Guo, Spherical polyelectrolyte brushes as a nanoreactor for synthesis of ultrafine magnetic nanoparticles, Nanotechnology 23 (2012) 265601–265610.

[30] W.S. Choi, H.Y. Koo, J.H. Park, D.Y. Kim, Synthesis of two types of nanoparticles in polyelectrolyte capsule nanoreactors and their dual functionality, JACS 127 (2005) 16136–16142.

[31] I. Willerich, F. Gröhn, Thermodynamics of Photoresponsive Polyelectrolyte? Dye Assemblies with Irradiation Wavelength Triggered Particle Size, Macromolecules 44 (11) (2011) 4452–4461.

[32] I. Willerich, F. Gröhn, Influencing Particle Size and Stability of Ionic Dendrimer-Dye Assemblies, J. Phys. Chem. B 114 (2010) 15466–15476.

[33] I.H. Willerich Ritter, F. Gröhn, Structure and Thermodynamics of Ionic Dendrimer-Dye Assemblies, J. Phys. Chem. B 113 (2009) 3339–3354.

[34] I. Willerich, T. Schindler, F. Gröhn, Effect of Polyelectrolyte Architecture and Size on Macroion–Dye Assemblies, J. Phys. Chem. B 115 (32) (2011) 9710–9719.

[35] I. Willerich, D. Moldenhauer, R. Schweins, F. Gröhn, Elucidating Electrostatic Self-Assembly: Molecular Parameters as Key to Thermodynamics and Nanoparticle Shape, J. Am. Chem. Soc. 138 (2016) 1280–1293.

[36] I. Willerich, F. Gröhn, Molecular Structure Encodes Nanoscale Assemblies: Understanding Driving Forces in Electrostatic Self-Assembly, J. Am. Chem. Soc. 133 (2011) 20341–20356.

[37] B. Holms, J. Swenson, K. Buck, D. Rivera, Investigations of the interaction and phase transfer to a TiO_2 surface of water soluble dyes with

polyelectrolyte/surfactant complexes using ultraviolet-visible spectroscopy and multivariate least squares analysis, Colloids Surf. A 404 (2012) 36–46.

[38] K. Hayakawa, R. Tanaka, J. Kurawaki, Y. Kusumoto, I. Satake, Thermodynamics of the Solubilization of Water-Insoluble Dyes by Complexes of Cationic Surfactants with Poly(vinyl sulfate) of Different Charge Densities, Langmuir 15 (1999) 4213–4216.

[39] M. Zhao, N.S. Zacharia, Sequestration of Methylene Blue into Polyelectrolyte Complex Coacervates, Macromol. Rapid Commun. 37 (2016) 1249–1255.

[40] F. Würthner, T.E. Kaiser, C.R. Saha-Möller, J-Aggregates: From Serendipitous Discovery to Supramolecular Engineering of Functional Dye Materials, Angew. Chem. Int. Ed. 50 (2011) 3376–3410.

[41] P.G. Tratnyek, T.E. Reilkoff, A.W. Lemon, M.M. Scherer, B.A. Balko, L.M. Feik, B.D. Henegar, Visualizing redox chemistry: probing environmental oxidation-reduction reactions with indicator dyes, Chem. Educator (2001) 172–179.

[42] F. Caruso, E. Donath, H. Möhwald, R. Georgieva, Fluoresence studies of the binding of anionic derivatives of pyrene and fluorescein to cationic polyelectrolytes in aqueous solution, Macromolecules 31 (1998) 7365–7377.

[43] D.A. Bryce, K.P. Kitt, J.M. Harris, Confocal Raman Microscopy Investigation of Molecular Transport into Individual Chromatographic Silica Particles, Anal. Chem. 89 (2017) 2755–2763.

[44] H. Eyring, The Activated Complex in Chemical Reactions, J. Chem. Phys. 3 (1935) 107–115.

[45] H. Seeboth, The Bucherer Reaction and the Preparative Use of its Intermediate Products, Angew. Chem. Int. Ed. 6 (1967) 307–317.

[46] H.M. Taylor, C.R. Hauser, α-(N,N Dimethylamino)phenylacetonitrile, Org. Synth. Coll. 5 (1973) 437.

 http://dx.doi.org/10.1016/j.heliyon.2017.e00397